LIP-STUDENTS-25-00

# Gravitational Waves from Supercooled Dark Conformal Phase Transitions

Vítor Alves[1,a]

[1] *Departamento de Física, Escola de Ciências, Universidade do Minho, 4710-057 Braga, Portugal*

Project supervisor: António P. Morais

*September 30, 2025*

**Abstract.** We investigate the dynamics of first-order phase transitions (FOPTs) in a classically scale-invariant dark sector featuring a single scalar field coupled to a hidden gauge symmetry. Radiative breaking of conformal invariance occurs through the Coleman–Weinberg mechanism, while renormalization-group (RG) improvement ensures a consistent treatment of quantum corrections. Finite-temperature effects, including daisy resummation, generate a thermal barrier that drives a strongly supercooled phase transition. We analyze the resulting effective potential at small field values, highlighting the emergence of shallow minima relevant for low-frequency gravitational waves detectable by pulsar timing arrays. From the effective potential we extract the critical, nucleation, and percolation temperatures, as well as key transition parameters ($\alpha$, $\beta/H$). These are then used to compute the stochastic gravitational-wave background (SGWB) spectrum, allowing for a comparison with current PTA hints (NANOGrav, EPTA). Our results show that conformal dark sectors provide a minimal and predictive framework capable of connecting radiative symmetry breaking, cosmological phase transitions, and low-frequency gravitational-wave signals.

Keywords: Conformal symmetry, Coleman–Weinberg potential, first-order phase transitions, stochastic gravitational-wave background, pulsar timing arrays

## 1 Introduction

The Standard Model (SM) of particle physics is one of the most successful theoretical frameworks in science, providing a precise description of fundamental particles and their interactions. It accurately explains three of the four fundamental forces, electromagnetic, weak, and strong, and has been experimentally confirmed with remarkable precision, most notably with the discovery of the Higgs boson in 2012 [1]. Despite these successes, the SM remains incomplete. It fails to account for several key phenomena, such as the origin of neutrino masses, the nature of dark matter, and the baryon asymmetry of the Universe. These shortcomings strongly motivate the search for new physics (NP) beyond the SM.

Gravitational waves (GWs) have emerged as a promising tool in this endeavor. Unlike photons, which decoupled only after the Universe became transparent, GWs can propagate freely from the earliest moments of cosmic history, carrying information about epochs otherwise inaccessible. The detection of a stochastic gravitational wave background (SGWB) would thus open a new observational window on the physics of the early Universe.

Recently, pulsar timing arrays (PTAs) have reported evidence for an SGWB at nanohertz frequencies [2, 3]. Although astrophysical sources such as supermassive black hole binaries (SMBHBs) provide a natural explanation, statistical analyzes suggest that NP scenarios may better account for the observed signal [4]. Among the most compelling candidates are strongly supercooled first-order phase transitions (FOPTs) occurring at MeV scales, which can efficiently produce gravitational waves compatible with the PTA data [5].

However, concerns have been raised about the viability of such scenarios. In particular, it has been argued that strongly supercooled FOPTs in models with SM-like scalar potentials may not fully complete on cosmological timescales, or may reheat the Universe to temperatures that shift the GW spectrum outside the PTA frequency range [6]. These conclusions are based on assumptions tied to electroweak-like models with cubic scalar interactions at tree level. This raises the question of whether such constraints hold in models with conformal dynamics.

This project focuses on the production of a stochastic gravitational wave background (SGWB) during strongly supercooled first-order phase transitions (FOPTs) in classically scale-invariant, or conformal, models. In these models, the scalar potential exhibits classical scale invariance, and breaking of this symmetry generates a pseudo-Goldstone boson (the scalon). A distinctive feature of such FOPTs is that the Universe can remain in a metastable phase for an extended period, releasing substantial latent heat and producing strong GW signals.

We will study scalar potentials associated with new gauge symmetries, analyze their vacuum structure and phase transitions, and compute the resulting GW spectra. These predictions will be compared with the sensitivity of current PTA experiments, such as NANOGrav and EPTA, while taking into account renormalization-group improvements and finite-temperature effects on the phase-transition dynamics.

## 2 Dark conformal scalar: potential, one-loop corrections and RG improvement

### 2.1 Dark Sector Setup and Potential

Dark sectors can in general couple to the Standard Model via portal interactions, such as the Higgs portal [7], or feature scalar multiplets with nontrivial representations under

[a] e-mail: pg59518@alunos.uminho.pt

some dark gauge symmetry [8]. Such features can enrich the phenomenology, introducing additional degrees of freedom and interactions that affect the structure of the effective potential and the dynamics of symmetry breaking.

In this work, however, we focus on a minimal and self-contained classically scale-invariant dark sector. In our construction, we deliberately omit any portal coupling to the Standard Model and consider only a single real scalar degree of freedom, denoted by $S$, representing the radial component of a hypothetical dark scalar field. No additional components of a multiplet are present and no other fields are dynamically relevant for the phase transition. This choice allows us to study in a clean and controlled way the structure of the effective potential and the radiative and thermal effects induced by the dark sector alone.

Classical scale invariance forbids any dimensionful parameters at tree level. Consequently, the tree-level potential along the dark scalar direction is purely quartic. The most general renormalizable potential consistent with scale invariance in this single-field setup reads

$$V_0(S) = \frac{\lambda_1}{8} S^4, \tag{1}$$

where $\lambda_1$ is a dimensionless quartic coupling and the normalization $1/8$ is chosen for later convenience [9].

### 2.2 Field-dependent masses

In the dark sector model considered here, the only relevant degrees of freedom are the scalar radial mode $S$ and the dark gauge bosons $X$. These gauge bosons acquire masses proportional to the scalar field value via the Higgs mechanism in the dark sector [10]. For a dark gauge boson $X$ with gauge coupling $g_X$, the field-dependent mass reads

$$M_X^2(S) = g_X^2 S^2. \tag{2}$$

These field-dependent masses are crucial because they determine the leading quantum corrections to the effective potential. In particular, they enter the one-loop Coleman–Weinberg potential, which governs the radiative breaking of scale invariance in the dark sector [9, 11].

This setup yields two physical scalars: the Standard Model Higgs boson $h_1$ and a dark scalar boson, commonly referred to as the scalon $h_2$. The masses of these particles depend on the vacuum expectation values of the corresponding scalar fields and determine the dynamics of the dark sector during the phase transition, which in turn affects the resulting gravitational wave signals.

### 2.3 One-loop Coleman–Weinberg potential

Quantum corrections at one-loop in dimensional regularization yield the Coleman–Weinberg (CW) effective potential [9, 11]. In general,

$$V_{\rm CW}(S) = \frac{1}{64\pi^2} \sum_a n_a M_a^4(S) \left( \ln \frac{M_a^2(S)}{Q^2} - C_a \right), \tag{3}$$

where the index $a$ runs over particle species (vectors, fermions, scalars), $n_a$ counts degrees of freedom (positive for bosons, negative for fermions with the conventional general sign conventions absorbed into $n_a$), $Q$ is the renormalization scale and $C_a$ is a scheme-dependent constant (for vectors in $\overline{\rm MS}$ one uses $C_{\rm vector} = 5/6$, and for scalars/fermions $C = 3/2$).

Retaining only the dominant gauge-boson contribution and inserting Eq. (2) with $n_X = 3$ (three polarizations per massive vector), one obtains

$$V_{\rm CW}(S) = \frac{3\, g_X^4 S^4}{64\pi^2} \left( \ln \frac{g_X^2 S^2}{Q^2} - \frac{5}{6} \right). \tag{4}$$

Combined with the tree-level potential, this yields the one-loop zero-temperature effective potential

$$V_{\rm eff}^{(0)}(S) \;=\; \frac{\lambda_1}{8} S^4 + \frac{3 g_X^4 S^4}{64\pi^2} \left( \ln \frac{g_X^2 S^2}{Q^2} - \frac{5}{6} \right), \tag{5}$$

which will be our working one-loop zero-temperature effective potential (tree-level + CW gauge contribution).

### 2.4 Tadpole condition and RG-improved potential

The extremum (tadpole) condition,

$$\left. \frac{\partial V_{\rm eff}^{(0)}(S)}{\partial S} \right|_{S=v_S} = 0, \tag{6}$$

establishes a direct relation between the quartic coupling $\lambda_1$ and the dark gauge coupling $g_X$ at the vacuum [9].

In the gauge-driven scenario considered here, retaining only the dominant gauge-boson contribution, $\lambda_1$ is radiatively generated by quantum corrections and can be approximated as

$$\lambda_1(S) \;\sim\; \frac{g_X^4 - 3\, g_X^4 \ln \frac{g_X^2 v_S^2}{Q^2}}{8\pi^2}, \tag{7}$$

indicating that the quartic arises entirely from the gauge-boson loop in the Coleman–Weinberg potential.

The scale dependence of $\lambda_1$ and $g_X$ is governed by the one-loop renormalization group equations (RGEs) [10, 11],

$$16\pi^2 \frac{dg_X}{dt} = \frac{1}{3} g_X^3, \qquad g_X(0) = g_0, \tag{8}$$

$$16\pi^2 \frac{d\lambda_1}{dt} = 6 g_X^4 - 12 g_X^2 \lambda_1 + 10 \lambda_1^2, \qquad \lambda_1(0) = \lambda_0, \tag{9}$$

where $t = \ln(\mu/\mu_0)$ is the logarithmic scale parameter, and $g_0$, $\lambda_0$ are the couplings on a reference scale $\mu_0$.

In the Coleman–Weinberg potential, Eq. (5), the logarithmic term involves the renormalization scale $Q$, which is identified with the RG scale $\mu$. At fixed one-loop order this leads to a spurious scale dependence, which is removed by promoting the couplings $g_X$ and $\lambda_1$ to running quantities governed by the RGEs above [9, 11].

The running couplings are then evaluated at a dynamical scale chosen to minimize large logarithmic corrections.

A convenient prescription, both at zero and finite temperature, is

$$\mu(S,T) = g_X(S)\,S. \tag{10}$$

Since RGEs admit closed-form analytic solutions in one loop, these can be substituted back into the Coleman–Weinberg potential. This procedure resums the leading logarithms and yields the RG-improved effective potential. A representative compact expression obtained by symbolic manipulation (CAS) is

$$V_{\rm RG}(S) = \frac{S^4(-24\pi^2\lambda_0 - 9g_0^4\ln(\frac{g_0 S}{\mu_0}) + g_0^2\lambda_0\ln(\frac{g_0 S}{\mu_0}))}{8(-24\pi^2 + g_0^2\ln(\frac{g_0 S}{\mu_0}))} + \frac{27g_0^4\pi^2 S^4\Big(-\frac{5}{6} + \ln\frac{24\pi^2}{24\pi^2 - g_0^2\ln(\frac{g_0 S}{\mu_0})}\Big)}{(24\pi^2 - g_0^2\ln(\frac{g_0 S}{\mu_0}))^2}. \tag{11}$$

Although the precise algebraic form depends on the renormalization convention, the essential point is that RG improvement can be implemented fully analytically at one loop, eliminating spurious scale dependence and consistently incorporating the leading quantum corrections into the dark-sector potential.

### 2.5 Finite-temperature corrections

To study cosmological phase transitions it is necessary to include thermal effects in the effective potential [11, 12]. At one loop, the finite-temperature contribution is given by

$$V_T(S,T) = \frac{T^4}{2\pi^2}\int_0^\infty dx\, x^2\,\ln\Big(1 - e^{-\sqrt{x^2 + M_X^2(S)/T^2}}\Big), \tag{12}$$

where $M_X(S)$ is the field-dependent mass of the dark gauge boson. In the present model, this is the only degree of freedom contributing, so the multiplicity factor is $n = 1$.

The integral in Eq. (12) can be expressed in terms of modified Bessel functions of the second kind [13], which is useful for analytical manipulations, or it can be evaluated numerically. For $M_X/T \ll 1$, high-temperature expansions provide reliable approximations, while for $M_X/T \gtrsim 1$ numerical evaluation is generally required.

Infrared divergences associated with bosonic Matsubara zero modes are cured by daisy resummation [12]. In the Arnold–Espinosa prescription, the daisy contribution reads

$$V_{\rm daisy}(S,T) = -\frac{T}{12\pi}\sum_b n_b\Big[(M_b^2(S) + \Pi_b(T))^{3/2} - (M_b^2(S))^{3/2}\Big]. \tag{13}$$

where $\Pi_X(T)$ is the temperature-dependent Debye mass of the gauge boson.

The full effective potential at finite temperature is then obtained by combining the zero-temperature contributions with $V_T$ and $V_{\rm daisy}$.

### 2.6 Finite-temperature effective potential and phase transition dynamics

The finite-temperature effective potential of the dark scalar can be written as

$$V_{\rm eff}(S,T) = V_{\rm RG}(S) + V_T(S,T) + V_{\rm daisy}(S,T), \tag{14}$$

This effective potential governs the dynamics of the phase transition relevant for low-frequency gravitational waves [14–16]. At temperatures around the MeV scale, it develops a barrier that separates the symmetric phase at the origin from the broken phase at a low VEV, making the transition first-order [17]. The barrier is entirely induced by the thermal effects of gauge bosons, while the zero-temperature potential determines the location of the true vacuum. The combined effect of these contributions is illustrated in Figs. 1-2.

Figure 1 shows the effective potential at relatively small field values for different temperatures. In this regime, which is relevant for the low-energy dynamics of the phase transition and thus for the generation of low-frequency gravitational waves, the appearance of a thermal barrier can be clearly seen [14]. As the temperature increases, the symmetric minimum at the origin is separated from the broken minimum by this barrier, signaling the onset of a first-order phase transition.

At slightly larger field values than those shown in Fig. 1, depicted in Fig. 2, thermal corrections become subdominant and the RG-improved zero-temperature potential dictates the vacuum structure [17]. The location of the true vacuum is essentially determined by the running of the couplings and is only mildly affected by finite-temperature contributions. Since this part of the potential sets the depth and stability of the broken phase, it controls the vacuum expectation value associated with symmetry

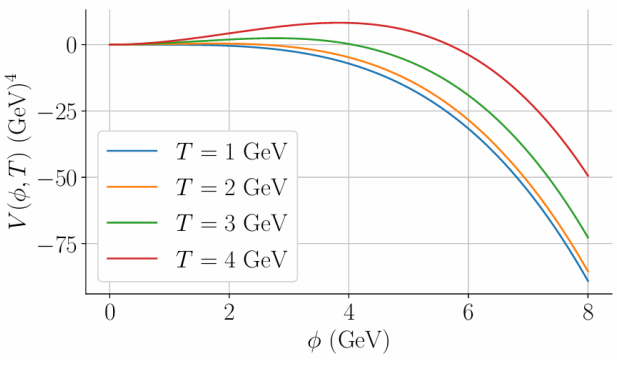


**Figure 1.** Finite-temperature effective potential $V_{\rm eff}(\phi, T)$ at small field values for several temperatures. The thermal barrier emerges as $T$ grows, a feature that governs the phase-transition dynamics and is directly connected to the production of low-frequency gravitational waves. The true vacuum is located at multi-TeV scales, corresponding to deeper potential wells and gravitational-wave signals in the frequency range accessible to space-based interferometers such as LISA, DECIGO, and BBO. Parameter values used for this plot are: $g_L = 0.677$, $\lambda_\sigma = 0.094$, $\lambda_h = 0.079$, $\lambda_{\sigma h} = 1.064 \times 10^{-33}$, $\mu_h = 4462.3$.

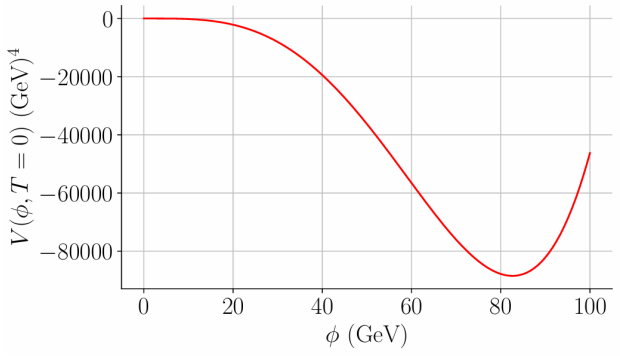


**Figure 2.** Snapshot of the effective potential for field values slightly larger than those in Fig. 1. The true vacuum is primarily set by the RG-improved zero-temperature potential and is only mildly affected by thermal corrections. This stabilizes the broken phase while maintaining a potential depth relevant for low-frequency gravitational-wave production. Parameter values used for this plot are: $g_L = 0.677$, $\lambda_\sigma = 0.094$, $\lambda_h = 0.079$, $\lambda_{\sigma h} = 1.064 \times 10^{-33}$, $\mu_h = 4462.3$

breaking. In the low-frequency regime, this ensures that the minimum is located at comparatively low values of the potential, consistent with the generation of signals observable by pulsar timing arrays [2].

This low-energy potential forms the basis for computing the phase transition parameters relevant for PTAs: the critical temperature $T_c$, the nucleation temperature $T_n$, the percolation temperature $T_p$, the transition strength $\alpha$, and the inverse time-scale $\beta/H$ [14, 16]. These quantities control the dynamics of the transition and determine the spectrum of the stochastic gravitational wave background (SGWB) in the nHz regime [2, 17].

In this work, we focus on signals accessible to pulsar timing arrays. The thermal potential presented here not only sets the vacuum structure of the dark scalar sector at low-energy scales but also provides the crucial link between microphysical dynamics and low-frequency cosmological signals [14, 15].

## 3 Gravitational-Wave Observables from First-Order Phase Transitions

The finite-temperature effective potential $V_{\rm eff}(\phi, T)$ governs the dynamics of first-order phase transitions (FOPTs) in the early Universe and determines the thermodynamic parameters that control the resulting low-frequency stochastic gravitational wave background (SGWB). These key quantities include the critical temperature $T_c$, at which the symmetric and broken minima are degenerate, the nucleation temperature $T_n$, when bubble nucleation becomes efficient, the percolation temperature $T_p$, which marks the epoch at which the expanding bubbles of true vacuum become causally connected, the transition strength $\alpha$, and the inverse time scale of the transition $\beta$ [15, 18].

The three-dimensional Euclidean bounce action $S_3(T)$ is obtained by solving

$$\frac{d^2\phi_b}{dr^2} + \frac{2}{r}\frac{d\phi_b}{dr} = \frac{dV_{\rm eff}(\phi_b, T)}{d\phi_b}, \qquad \frac{d\phi_b}{dr}\Big|_{r=0} = 0, \quad \phi_b \to 0 \text{ as } r \to \infty \tag{15}$$

After obtaining the bubble profile, one can calculate the three-dimensional action $S_3(T)$, defined as [19][**?** ]:

$$S_3(T) = 4\pi \int_0^\infty dr\, r^2 \left[\frac{1}{2}\left(\frac{d\phi_b}{dr}\right)^2 + V_{\rm eff}(\phi_b, T)\right]. \tag{16}$$

with the decay rate of the false vacuum given by

$$\Gamma(T) = A(T)\, e^{-S_3(T)/T}, \quad A(T) \sim T^4 \left(\frac{S_3}{2\pi T}\right)^{3/2}. \tag{17}$$

The nucleation temperature satisfies

$$\int_{T_n}^{T_c} \frac{dT}{T} \frac{\Gamma(T)}{H(T)^4} = 1, \tag{18}$$

while the percolation temperature $T_p$ ensures completion of the phase transition. The transition strength $\alpha$ quantifies the ratio between the latent heat density, $L_H$, and the total radiation energy density, and also indicates whether the phase transition is supercooled. These quantities are defined as [17]

$$L_H = -\Delta F - T\Delta S = \Delta V - T\frac{\partial \Delta V}{\partial T}, \tag{19}$$

$$\alpha = \frac{L_H}{\rho_{\rm rad}} = \frac{\Delta V - T\frac{\partial \Delta V}{\partial T}}{\rho_{\rm rad}}\Big|_{T=T_p}, \tag{20}$$

where $\Delta F$ is the difference in free energy between the two minima, $\Delta S$ the corresponding entropy difference, and $g^* = 106.75$ is the number of degrees of freedom in the plasma.

After defining the transition strength, the inverse time scale of the phase transition, $\beta$, can be determined from the rate of bubble nucleation, $\Gamma(t) \sim e^{\beta t}$. Expanding the three-dimensional Euclidean action $S_3(T)$ around a reference time $t'$ gives the following result.

$$\frac{S_3}{T}(t) \simeq \frac{S_3}{T}(t') + \frac{d}{dt}\frac{S_3}{T}\Big|_{t=t'} (t - t') + O((t - t')^2), \tag{21}$$

leading to

$$\beta = -\frac{d}{dt}\frac{S_3(T)}{T}\Big|_{t=t'} \quad \Longrightarrow \quad \frac{\beta}{H'} = T\frac{d}{dT}\frac{S_3(T)}{T}\Big|_{T=T_p}, \tag{22}$$

where $H'$ is the Hubble rate at the time of the transition and $dT/dt = -TH'$. [20]

The characteristic length scale of the transition, $R_*$, can be estimated as the radius of the bubble at percolation:

$$H'R_* \simeq (8\pi)^{1/3}\frac{1}{\beta/H'}. \tag{23}$$

At this stage, the dynamics of bubble expansion and collisions determine how the energy released during the

phase transition is converted into gravitational waves. Gravitational waves (GWs) are generated by the expansion and collision of bubbles of a true vacuum. Depending on the bubble dynamics, two mechanisms dominate. If the bubble wall reaches a terminal velocity due to interactions with the plasma before collision, the primary source is the sound waves in the fluid, which convert a fraction $\kappa_{\rm SW}$ of the vacuum energy into kinetic energy. In strongly supercooled transitions at low temperatures relevant for pulsar timing arrays (nHz range), bubble walls can accelerate almost freely, concentrating most of the energy in the wall itself. In this case, dominant GW source is bubble collisions, with the efficiency factor $\kappa_{\rm BC}$ determined by the ratio of the bubble-wall energy to the total released vacuum energy [16, 21].

The peak frequency $f_{\rm peak}$ and amplitude $\Omega_{\rm GW}^{\rm peak}$ of the resulting stochastic gravitational wave background (SGWB) can be expressed in terms of the thermodynamic parameters, the characteristic bubble size $R_*$ in percolation, and the Hubble expansion in the transition. For low-frequency transitions, sound waves are typically subdominant, but the formalism including double broken power laws for sound waves and single broken power law for bubble collisions remains valid [14, 15].

For the calculation of the SGWB peak amplitude $\Omega_{\rm GW}^{\rm peak}$ and frequency $f_{\rm peak}$, the contributions of bubble-wall collisions and sound waves are modeled using power-law templates. For bubble collisions, a single broken power law is adopted, while for sound waves, a double broken power law is used [14, 22]. The geometric parameters of the spectrum are related to the thermodynamic properties of the phase transition:

$$h^2\Omega_{\rm BC}^{\rm peak} \simeq \tilde{K}^2\left(\frac{H_*}{\beta}\right)^2, \qquad f_{\rm BC}^{\rm peak} \simeq \frac{\beta}{H(T_p)}, \tag{24}$$

$$h^2\Omega_{\rm SW}^{\rm peak} \simeq K^2\left(\frac{H_*}{\beta}\right), \qquad f_{\rm SW}^{\rm peak} \simeq \frac{\beta}{H(T_p)}, \tag{25}$$

where $K \simeq 0.6\,\kappa_{\rm SW}\alpha/(1+\alpha)$ and $\tilde{K} \equiv \kappa_{\rm BC}\alpha/(1+\alpha)$ are the fractional energy densities converted into sound waves and bubble-wall motion, respectively [22]. $H_*$ is the Hubble parameter at percolation, $R_*$ the characteristic bubble size, and $\beta/H(T_p)$ parameterizes the inverse time scale of the transition. These expressions highlight that $\Omega_{\rm GW}^{\rm peak}$ scales quadratically with the energy fraction for bubble collisions and linearly for sound waves, whereas $f_{\rm peak}$ is primarily set by the rate of bubble nucleation and expansion.

This parameterization allows one to directly map the thermodynamic features of a first-order phase transition, namely $\alpha$, $\beta/H$, and $R_*$, onto the expected gravitational wave signal in the nHz regime relevant for pulsar timing arrays, where strongly supercooled transitions dominate the SGWB signal via bubble collisions [16, 21].

Low-frequency GWs, accessible to pulsar timing arrays, are sensitive to strongly supercooled first-order phase transitions at MeV scales, where bubble collisions dominate the signal, whereas higher-frequency signals, observable by space-based interferometers such as LISA and DECIGO, are not considered here. The interplay between transition strength, supercooling, and bubble dynamics determines the SGWB signal in the nHz range, with sound waves typically being subdominant. This framework establishes a direct connection between the thermal effective potential of the dark scalar and the low-frequency gravitational-wave signals potentially observable by pulsar timing arrays.

## 4 Numerical results

We now focus on the parameter space relevant for low-frequency gravitational-wave (GW) signals, accessible to pulsar timing arrays (PTAs) [4]. In our scenario, the dark conformal sector undergoes a first-order phase transition (FOPT) at MeV-scale temperatures, generating a stochastic gravitational wave background (SGWB) in the nHz frequency band [17]. Numerical scans were performed with the scalar mass parameter $M_{h_2}$ sampled logarithmically in the range $[0.01, 100]$ MeV and the gauge coupling $g_L$ varied linearly within $[0.20, 1.25]$.

Within these ranges, we analyze the dependence of key parameters, $g_L$, scalar self-coupling $\lambda_\sigma$, transition strength $\alpha$, and inverse time scale $\beta/H$, on the amplitude and peak frequency of the SGWB.

These correlations determine which regions of parameter space produce signals observable by current and future PTA experiments, as illustrated in Figs. 3–6.

Figures 3–6 illustrate scatter plots of the SGWB peak amplitude versus peak frequency for each parameter. The gauge coupling $g_L$, shown in Fig. 3, primarily influences the peak amplitude: smaller values of $g_L$ result in larger amplitudes, reflecting the deeper vacuum at the true minimum of the effective potential. Similarly, the scalar self-coupling $\lambda_\sigma$, shown in Fig. 4, shows a strong correlation with the peak amplitude. Smaller magnitudes of $\lambda_\sigma$ enhance the GW signal by increasing the degree of supercooling while avoiding extreme vacuum domination [17].

The transition strength $\alpha$, depicted in Fig. 5, quantifies the ratio of latent heat to the density of radiation energy at percolation temperature $T_p$ [14, 15]. In our MeV-scale FOPTs, $\alpha$ remains below the extreme supercooling threshold ($\alpha \lesssim 10^8$), ensuring that the reheating does not exceed the dark sector mass scale and the GW spectrum remains in the PTA band [17]. Finally, the inverse time scale $\beta/H$, shown in Fig. 6, determines the characteristic duration of the phase transition and, consequently, the width of the GW spectrum. Faster transitions (larger $\beta/H$) lead to narrower spectral features.

In general, these results indicate that low-frequency GW signals in the nHz regime can be generated by MeV-scale FOPTs in the dark conformal sector, with the peak amplitude and spectral features controlled by $g_L$, $\lambda_\sigma$, $\alpha$ and $\beta/H$. The correlations observed among these parameters provide clear guidance for selecting regions of parameter space capable of producing signals observable by current and future pulsar timing array experiments.

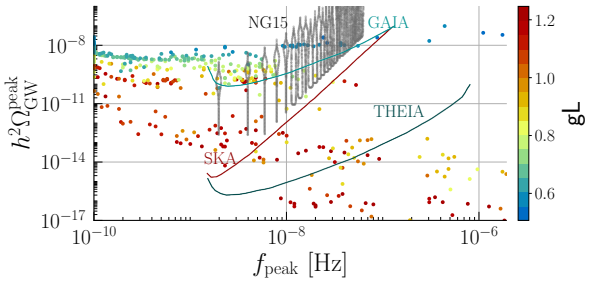


**Figure 3.** Scatter plot of SGWB peak amplitude versus peak frequency as a function of gauge coupling $g_L$. Smaller couplings result in higher amplitudes at lower frequencies relevant for PTAs.

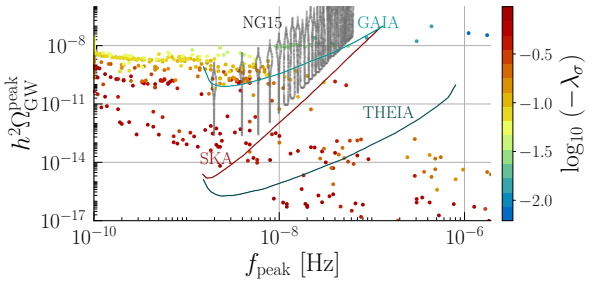


**Figure 4.** Scatter plot of SGWB peak amplitude versus peak frequency for the scalar self-coupling $\lambda_\sigma$. Smaller magnitudes enhance the GW amplitude by increasing supercooling.

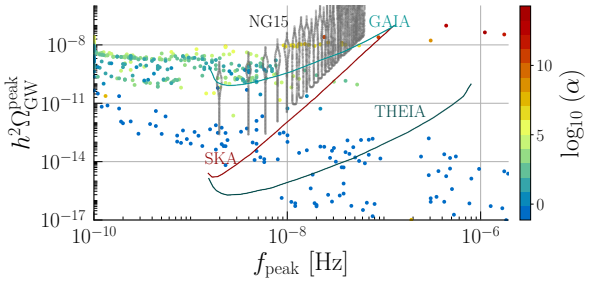


**Figure 5.** Transition strength $\alpha$ as a function of SGWB peak frequency. Values remain below the extreme supercooling threshold, ensuring that reheating does not exceed the dark sector mass scale.

## 5 Conclusions

In this work we have constructed and analyzed the effective potential of a conformal dark sector, where radiative symmetry breaking arises via the Coleman-Weinberg mechanism and is consistently treated through renormalization-group improvement. By including finite-temperature corrections and daisy resummation, we demonstrated how a thermal barrier emerges, triggering a strongly first-order phase transition.

The analysis of the effective potential across different field regimes revealed that shallow minima at low field values lead to gravitational-wave signals in the

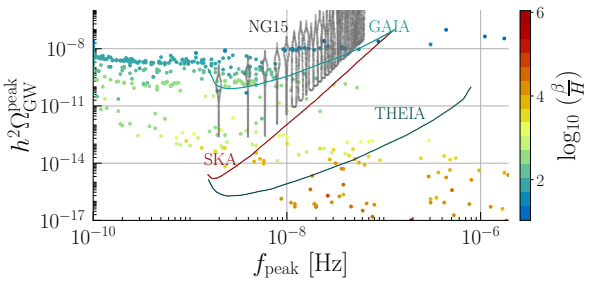


**Figure 6.** Inverse time-scale $\beta/H$ versus SGWB peak frequency. Larger $\beta/H$ corresponds to faster transitions and narrower GW spectra.

nanohertz band, relevant for pulsar timing array experiments. Higher-scale minima and millihertz signals are not considered here, as the focus is on low-frequency GW production. This establishes a natural connection between early Universe dynamics and low-frequency gravitational wave observations.

From the effective potential, we extracted the characteristic phase transition parameters, including the critical, nucleation, and percolation temperatures, as well as $\alpha$ and $\beta/H$. These quantities determine the strength and spectral characteristic of the stochastic gravitational wave background in the nHz range, allowing for a direct comparison with current PTA hints such as NANOGrav, EPTA, and other low-frequency observatories.

In general, the results show that minimal conformal dark sectors provide a predictive and testable framework for supercooled cosmological phase transitions that produce low-frequency gravitational waves. The focus on PTA-accessible signals highlights the potential of these models to connect particle physics and low-frequency gravitational-wave cosmology. Future refinements, such as higher-loop corrections and non-perturbative analyses, will be valuable to reduce theoretical uncertainties, but the key qualitative features and observational prospects identified here are robust.

## Acknowledgements

The author would like to express his deepest gratitude to Prof. António P. Morais for his invaluable guidance, insightful discussions, and continuous supervision throughout the development of this project. Special thanks are also due to João Gonçalves for his helpful advice and support during different stages of this work. Finally, the author acknowledges LIP (Laboratório de Instrumentação e Física Experimental de Partículas) for the opportunity to carry out this internship and for providing a stimulating research environment.

## References

[1] G. Aad, T. Abajyan, B. Abbott, J. Abdallah, S. Abdel Khalek, A. Abdelalim, O. Abdinov, R. Aben,

B. Abi, M. Abolins et al., Physics Letters B **716**, 1–29 (2012)

[2] G. Agazie, A. Anumarlapudi, A.M. Archibald, Z. Arzoumanian, P.T. Baker, B. Bécsy, L. Blecha, A. Brazier, P.R. Brook, S. Burke-Spolaor et al., The Astrophysical Journal Letters **951**, L8 (2023)

[3] B. Goncharov, R.M. Shannon, D.J. Reardon, G. Hobbs, A. Zic, M. Bailes, M. Curyło, S. Dai, M. Kerr, M.E. Lower et al., The Astrophysical Journal Letters **917**, L19 (2021)

[4] A. Afzal, G. Agazie, A. Anumarlapudi, A.M. Archibald, Z. Arzoumanian, P.T. Baker, B. Bécsy, J.J. Blanco-Pillado, L. Blecha, K.K. Boddy et al., The Astrophysical Journal Letters **951**, L11 (2023)

[5] A. Gonstal, M. Lewicki, B. Swiezewska, *Reconstructing early universe evolution with gravitational waves from supercooled phase transitions* (2025), 2502.18436, https://arxiv.org/abs/2502.18436

[6] C.T.L.L.M.L.W.Y.W.Z.X. P. Athron, A. Fowlie, Phys. Rev. Lett. (2024)

[7] B. Patt, F. Wilczek, *Higgs-field portal into hidden sectors* (2006), hep-ph/0605188, https://arxiv.org/abs/hep-ph/0605188

[8] B. Dutta, D. Goswami, A. Karthikeyan, *Monophotons from scalar portal dark matter at neutrino experiments* (2025), 2507.07936, https://arxiv.org/abs/2507.07936

[9] E.J. Weinberg, *Radiative corrections as the origin of spontaneous symmetry breaking* (2005), hep-th/0507214, https://arxiv.org/abs/hep-th/0507214

[10] M. Peskin, D. Schroeder, *An Introduction to Quantum Field Theory* (Addison-Wesley, 1995)

[11] M. Quiros, *Finite temperature field theory and phase transitions* (1999), hep-ph/9901312, https://arxiv.org/abs/hep-ph/9901312

[12] P. Arnold, O. Espinosa, Phys. Rev. D **47**, 3546 (1993)

[13] L. Dolan, R. Jackiw, Phys. Rev. D **9**, 3320 (1974)

[14] C. Caprini, M. Hindmarsh, S. Huber, T. Konstandin, J. Kozaczuk, G. Nardini, J.M. No, A. Petiteau, P. Schwaller, G. Servant et al., Journal of Cosmology and Astroparticle Physics **2016**, 001–001 (2016)

[15] D.J. Weir, Philosophical Transactions of the Royal Society A: Mathematical, Physical and Engineering Sciences **376**, 20170126 (2018)

[16] M. Hindmarsh, S.J. Huber, K. Rummukainen, D.J. Weir, Physical Review D **92** (2015)

[17] M. Breitbach, *Gravitational waves from cosmological phase transitions* (2022), 2204.09661, https://arxiv.org/abs/2204.09661

[18] C. Caprini, Journal of Physics: Conference Series **610**, 012004 (2015)

[19] S. Coleman, Phys. Rev. D **15**, 2929 (1977)

[20] P. Athron, C. Balázs, L. Morris, Journal of Cosmology and Astroparticle Physics **2023**, 006 (2023)

[21] J.R. Espinosa, T. Konstandin, J.M. No, G. Servant, Journal of Cosmology and Astroparticle Physics **2010**, 028 (2010)

[22] C. Caprini, R. Jinno, M. Lewicki, E. Madge, M. Merchand, G. Nardini, M. Pieroni, A.R. Pol, V. Vaskonen, for the LISA Cosmology Working Group, Journal of Cosmology and Astroparticle Physics **2024**, 020 (2024)